Rhinovirus induces an anabolic reprogramming in host cell metabolism essential for viral replication

Guido A. Gualdoni[a,b,1], Katharina A. Mayer[a], Anna-Maria Kapsch[a,c], Katharina Kreuzberg[a], Alexander Puck[a], Philip Kienzl[d], Felicitas Oberndorfer[e], Karin Frühwirth[f], Stefan Winkler[f], Dieter Blaas[g], Gerhard J. Zlabinger[a], and Johannes Stöckl[a]

[a]Institute of Immunology, Center of Pathophysiology, Immunology & Infectiology, Medical University of Vienna, 1090 Vienna, Austria; [b]Division of Nephrology and Dialysis, Department of Medicine 3, Medical University of Vienna, 1090 Vienna, Austria; [c]Global Pathogen Safety, Shire, 1090 Vienna, Austria; [d]Division of Immunology, Allergy and Infectious Diseases, Department of Dermatology, Medical University of Vienna, 1090 Vienna, Austria; [e]Department of Pathology, Medical University of Vienna, 1090 Vienna, Austria; [f]Division of Infectious Diseases and Tropical Medicine, Department of Medicine 1, Medical University of Vienna, 1090 Vienna, Austria; and [g]Department of Medical Biochemistry, Max F. Perutz Laboratories, Vienna Biocenter, Medical University of Vienna, 1090 Vienna, Austria

Edited by Peter Palese, Icahn School of Medicine at Mount Sinai, New York, NY, and approved June 21, 2018 (received for review January 10, 2018)

Rhinoviruses (RVs) are responsible for the majority of upper airway infections; despite their high prevalence and the resulting economic burden, effective treatment is lacking. We report here that RV induces metabolic alterations in host cells, which offer an efficient target for antiviral intervention. We show that RV-infected cells rapidly up-regulate glucose uptake in a PI3K-dependent manner. In parallel, infected cells enhance the expression of the PI3K-regulated glucose transporter GLUT1. In-depth metabolomic analysis of RV-infected cells revealed a critical role of glucose mobilization from extracellular and intracellular pools via glycogenolysis for viral replication. Infection resulted in a highly anabolic state, including enhanced nucleotide synthesis and lipogenesis. Consistently, we observed that glucose deprivation from medium and via glycolysis inhibition by 2-deoxyglucose (2-DG) potently impairs viral replication. Metabolomic analysis showed that 2-DG specifically reverts the RV-induced anabolic reprogramming. In addition, treatment with 2-DG inhibited RV infection and inflammation in a murine model. Thus, we demonstrate that the specific metabolic fingerprint of RV infection can be used to identify new targets for therapeutic intervention.

rhinovirus | metabolism | metabolomics | antiviral therapy

In the absence of a self-contained metabolism, viruses depend on the host cell to provide components for their rapid reproduction. To cope with the resulting elevated bioenergetic demands, viruses have evolved strategies to dramatically modify nutrient uptake as well as biosynthetic pathways of the host cells (1).

In most cases of energetic homeostasis, ATP production is maintained by glycolysis, TCA cycle, and oxidative phosphorylation. However, in highly anabolic states, glutamine serves as the predominant extracellular carbon source. It is utilized in an anaplerotic reaction in the TCA cycle as a substitute for glucose, which is required for anabolic processes such as fatty acid synthesis and nucleotide generation (2, 3).

This key platform of energy and macromolecule supply is a major target for viral metabolic intervention. Although there are similarities among the virus-triggered metabolic alterations to some extent, distinct modifications with respect to the preferred carbon source and the primarily targeted biosynthetic pathways were observed depending on the specific infectious agent (1). For instance, vaccinia virus as well as cytomegalovirus depend on an increase in glutamine uptake (4, 5), whereas other viruses enhance glucose uptake for energy generation and biosynthesis (6–8). Regarding the molecular mechanisms leading to these alterations, Thai et al. (9, 10) recently identified the transcription factor MYC to be of critical relevance for glucose as well as glutamine pathway alterations upon adenoviral infection.

Rhinoviruses (RVs) are ssRNA-nonenveloped viruses that belong to the family of Picornaviridae. They are responsible for more than 50% of upper airway infections and cause several billion dollars of health care costs per year (11–13). Apart from causing the common cold, they trigger lower respiratory tract infections in immunosuppressed patients (14, 15), chronic obstructive pulmonary disease, and asthma exacerbations (16, 17). To date, there is no available treatment for RV infections.

Despite the relevance of the virus in human pathogenesis, knowledge on the interaction of RV and the host cell metabolism is limited.

In this study, we sought to elucidate the metabolic implications of RV infection. We observed that viral infection led to extensive alterations of cellular metabolism and enhanced expression of enzymes responsible for glucose utilization and uptake. Indeed, the shift toward a glucose-dependent anabolic state is of vital importance for the viral infection, as evidenced by the abolishment of viral replication upon glucose deprivation and glycolysis inhibition. Last, we delineated a mode of metabolism-targeting antiviral therapy in vitro and in vivo by using the glycolysis inhibitor 2-deoxyglucose (2-DG).

Results

RV Infection Enhances Glucose Uptake. To investigate the impact of RV on host cell metabolism, we first assessed the kinetics of nutrient uptake in infected cells compared with controls. For this purpose, we exposed primary human fibroblasts and HeLa cells to fluorescently labeled glucose at different time points during RV-B14 infection. We found that RV infection led to an enhancement

Significance

Rhinovirus (RV) is the causative agent of the common cold and other respiratory tract infections. Despite the vast prevalence, effective treatment or prevention strategies are lacking. Here, we analyzed metabolic alterations in infected cells and found a pronounced reprogramming of host cell metabolism toward an anabolic state, which involved enhancement of glucose uptake and glycogenolysis. We further demonstrate that these alterations can be reverted by treatment with 2-deoxyglucose, a glycolysis inhibitor, which results in a disruption of RV replication in vitro and in vivo. Thus, we show how the specific metabolic fingerprint of viral infection can be used to generate targets for antiviral therapy.

Author contributions: G.A.G., G.J.Z., and J.S. designed research; G.A.G., K.A.M., A.-M.K., K.K., A.P., P.K., F.O., and K.F. performed research; P.K., S.W., D.B., G.J.Z., and J.S. contributed new reagents/analytic tools; G.A.G., K.A.M., K.K., A.P., F.O., D.B., and J.S. analyzed data; and G.A.G. and J.S. wrote the paper.

The authors declare no conflict of interest.

This article is a PNAS Direct Submission.

[1]To whom correspondence should be addressed. Email: guido.gualdoni@meduniwien.ac.at.

This article contains supporting information online at www.pnas.org/lookup/suppl/doi:10.1073/pnas.1800525115/-/DCSupplemental.

Published online July 9, 2018.

of glucose incorporation by the infected cells (Fig. 1 *A* and *B*). RV is known to activate the PI3K pathway (18–21), an essential platform in the modulation of metabolic homeostasis that is responsible for rapid adaptation of glucose uptake (22, 23). To test whether the activation of this pathway played a role in our observations, we analyzed the impact of the established PI3K inhibitors PP242 and LY294002 on RV-induced glucose uptake (24). Coincubation with any of the inhibitors during RV infection reverted the effect on glucose uptake, pointing toward an involvement of this pathway in our observations (Fig. 1*C*). In coherence with these findings, the expression of primarily PI3K-regulated enzyme GLUT1 was significantly enhanced after 1.5 h and 4 h of RV infection and went back to control levels at 7.5 h (Fig. 1 *D* and *E*). In line with a concept of PI3K orchestrating RV-induced effects, the expression of GLUT3 was not affected by RV infection, thus pointing toward a specific effect on PI3K-regulated targets (*SI Appendix*, Fig. S1*A*). In addition to glucose uptake, the uptake of fluorescently labeled fatty acids was also up-regulated during RV-B14 infection in HeLa cells (*SI Appendix*, Fig. S1*B*).

Taken together, these findings indicate an up-regulation of nutrient uptake by RV in fibroblasts and HeLa cells, which was dependent on PI3K. These alterations were accompanied by an enhanced expression of the PI3K-modulated enzyme GLUT1, potentially mediating the observed effects.

RV Induces an Anabolic State in Host Cell Metabolism. To further deepen our understanding of RV-induced metabolic alterations, we performed an MS-based analysis of biochemical compounds in HeLa cells during RV-B14 infection.

RV infection was associated with a marked increase in the levels of the glycogen metabolism intermediates maltotetraose, maltotriose, maltose, and UDP-glucose, indicating the activation of glycogenolysis (Fig. 2 and Dataset S1).

With respect to lipid metabolism, we found that the infected cells exhibited a significant decrease in the levels of various medium- and long-chain acylcarnitines, which suggests that infection decreases fatty acid oxidation. This change may reflect infection-induced metabolic reprogramming toward fatty acid synthesis and away from oxidation. Indeed, the concentrations of acetyl-CoA, oleoyl-CoA, and multiple long-chain and polyunsaturated fatty acids were significantly elevated, or at least showed such a trend, relative to uninfected control samples; several phospholipids, sphingolipids, ceramides, and the fatty acid synthase enzyme cofactor phosphopantetheine were also significantly increased, further suggesting a shift toward lipogenesis and/or fatty acid uptake (*SI Appendix*, Fig. S2 and Dataset S1).

Regarding the nucleotide metabolism, which is crucial for viral replication, we found that multiple nucleotide triphosphates and diphosphates, including guanosine 5′-triphosphate, guanosine 5′-diphosphate, uridine 5′-triphosphate, uridine 5′-diphosphate, CTP, and cytidine 5′-diphosphate, were significantly increased 7 h post infection relative to uninfected cells. Elevated nucleotide levels were accompanied by increased concentrations of ribulose 5-phosphate and xylulose 5-phosphate, which suggests the activation of the pentose phosphate pathway to synthesize nucleotide precursors (*SI Appendix*, Fig. S2 and Dataset S1).

Taken together, metabolomic analysis revealed an infection-induced reprogramming of the host cell metabolism toward anabolic processes by affecting carbohydrate, fatty acid, and nucleotide metabolism.

RV Depends on Glucose for Reproduction. Having identified the overall metabolic shift and enhancement of nutrient uptake

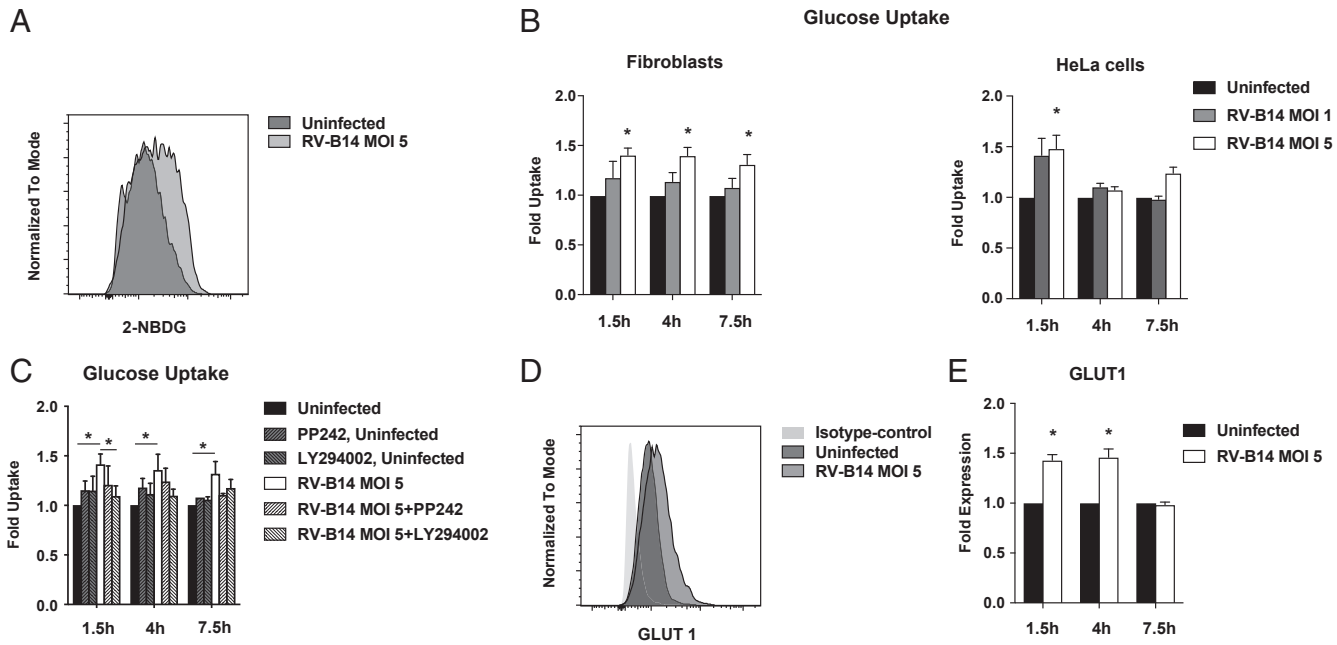

Fig. 1. RV infection enhances nutrient uptake and the expression of glucose transporters. (*A*) Representative measurement of the uptake of fluorescently labeled glucose (2-NBDG) in RV-B14–infected and uninfected primary human fibroblasts at 1.5 h post infection. (*B*) Mean ± SEM of the four experiments in fibroblasts and HeLa cells [$*P < 0.05$, paired *t* test of raw mean fluorescence intensity (MFI) data]. (*C*) Impact of the PI3K inhibitors LY294002 (10 μM) and PP242 (1 μM) on glucose uptake of RV-B14–infected fibroblasts ($*P < 0.05$, paired *t* test). (*D*) Representative measurement of GLUT1 expression in RV-B14–infected fibroblasts at 1.5 h post infection. (*E*) Mean ± SEM of the four experiments in fibroblasts ($*P < 0.05$, paired *t* test).

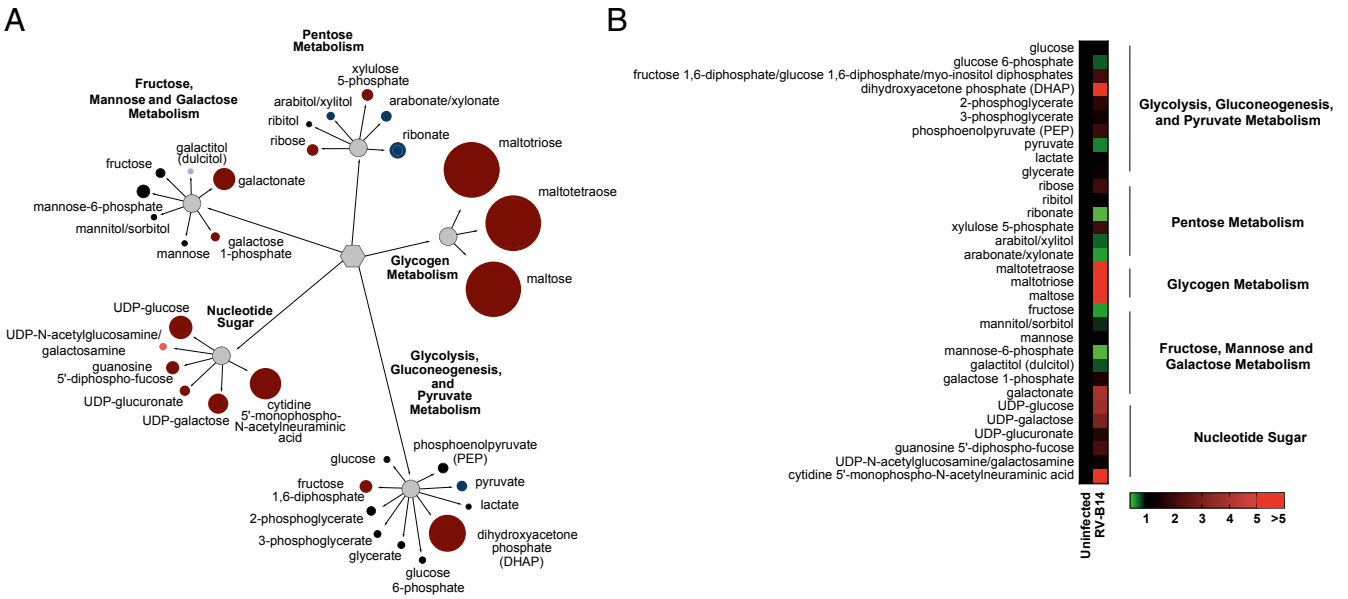

Fig. 2. RV induces an anabolic reprogramming of host cell metabolism. Metabolomic analysis of HeLa cells infected with RV-B14 (MOI of 3.5) at 7 h post infection. (*A*) The impact of RV infection on carbohydrate metabolism. Colored circles represent statistically significant changes. Dark red circles represent up-regulations; dark blue circles represent down-regulations with $P \leq 0.05$ and fold change >1. Bright red circles represent up-regulations; bright blue circles represent down-regulations with $0.05 < P < 0.10$ and fold change >1. The diameter of the circles represents the degree of change compared with uninfected cells. (*B*) Impact of RV on carbohydrate metabolism in heat map format.

during RV infection, we further evaluated the role of these processes in viral reproduction. We found that RV replication was impaired in glucose-depleted growth medium (Fig. 3*A*). Glucose deprivation from culture medium had no impact on cell viability (*SI Appendix*, Fig. S3), indicating a specific effect on viral reproduction. In certain anabolic states, glutamine is utilized in an anaplerotic reaction to feed the TCA cycle, and many viruses depend on this mechanism for proper reproduction (4, 5). Therefore, we also tested the impact of glutamine deprivation on RV replication. We found that glutamine deprivation also resulted in impaired RV replication, thus outlining the relevance of carbon supply for unhindered viral reproduction (Fig. 3*A*).

These findings indicate that RV infection not only induces a highly anabolic state and enhances nutrient uptake, but is also highly dependent on glucose for efficient replication.

The Glycolysis Inhibitor 2-DG Potently Impairs RV Replication. To further analyze the role of glucose metabolism during infection, we assessed the impact of the glycolysis inhibitor 2-DG on viral replication. In line with our previous findings, 2-DG strongly inhibited RV reproduction in HeLa cells and in primary human fibroblasts (Fig. 3*B*). Measurement of viral replication on the protein level (VP1-3 synthesis in HeLa cells) showed similar results as on the RNA level (Fig. 3*C*). The concentrations of 2-DG employed had no measurable impact on cell viability (*SI Appendix*, Fig. S4).

2-DG affects glycolysis at a very early stage through competitive inhibition of phosphoglucoisomerase (PGI), thereby not only affecting ATP generation but also impairing carbon flux through the TCA cycle to provide macromolecules for anabolic processes. We were interested to also assess the impact of downstream glycolysis inhibition. Therefore, we used oxamate, which impairs the formation of lactate from pyruvate and therefore abolishes anaerobic glycolysis without affecting the processing of pyruvate through the TCA cycle. In contrast to 2-DG, oxamate treatment had no impact on RV replication (Fig. 3*D*), suggesting a less consequential role of anaerobic glycolysis in RV reproduction.

Apart from its impact on glucose metabolism, 2-DG is known to interfere with N-linked glycosylation, thus causing endoplasmic reticulum stress and an unfolded protein response (UPR). These processes have been described to be involved in cellular antiviral responses (25). To assess whether this mechanism plays a role in our observations, we coincubated the infected cells treated with 2-DG along with mannose, which is an established antagonist of 2-DG–induced UPR (26). The antiviral activity of 2-DG was not affected by mannose treatment (*SI Appendix*, Fig. S5), which excludes the interference of protein glycosylation as an antiviral mechanism of 2-DG.

Additionally, we had seen that fatty acid uptake was up-regulated by RV infection (*SI Appendix*, Fig. S1*B*). The metabolomics data suggested that infection resulted in enhanced lipogenesis rather than fatty acid oxidation in infected cells (*SI Appendix*, Fig. S2 and Dataset S1). We used etomoxir, a specific inhibitor of fatty acid oxidation (27, 28), to study the role of this process in infected cells. In line with our previous observations, etomoxir had no impact on RV replication in HeLa cells (Fig. 3*E*).

Thus, we established a unique inhibitory property of 2-DG on RV infection by the inhibition of upstream glycolysis, whereas inhibition of neither fatty acid oxidation nor anaerobic glycolysis showed any impact on RV reproduction.

2-DG Reverts RV-Induced Reprogramming of Host Cell Metabolism. To acquire a better understanding of the mechanistic basis of 2-DG's antiviral effect, we performed metabolomic studies of cells infected with RV in the presence of this compound. Consistent with the concept of early glycolysis inhibition through PGI by 2-DG, the levels of early glycolysis intermediates such as glucose and glucose-6-phosphate were strongly enhanced by 2-DG treatment, whereas the levels of late-stage glycolytic products such as pyruvate and lactate were significantly decreased with 2-DG treatment (Fig. 4 and Dataset S1). Strikingly, 2-DG reversed many of the RV-induced modifications of cellular metabolism. RV-induced glycogenolysis was abolished by 2-DG treatment (Fig. 4). Regarding lipid metabolism, 2-DG treatment of the infected cells led to a significant increase in the levels of several

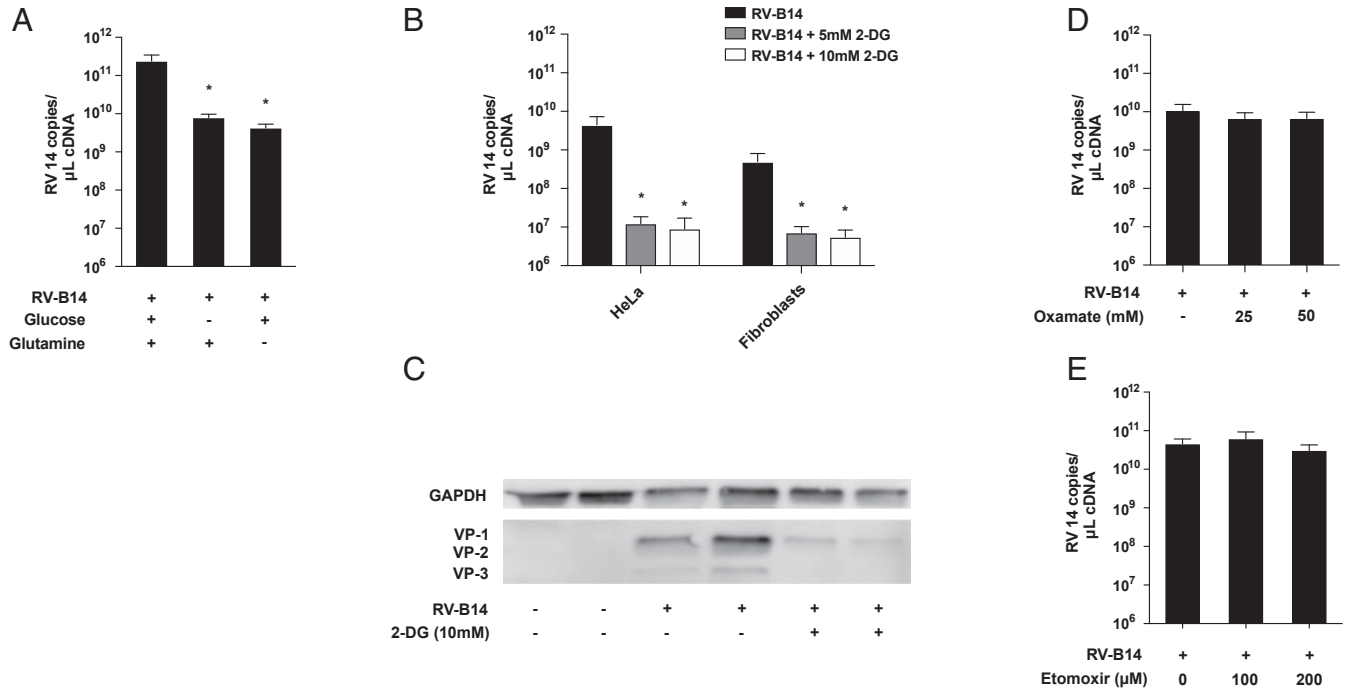

Fig. 3. Glucose deprivation is detrimental for RV replication. (*A*) RV-B14 replication in HeLa cells under glucose-deprived or glutamine-deprived conditions. Cells were infected in normal glucose and glutamine-containing medium, glucose-deprived medium, or glutamine-deprived medium. Analysis of viral RNA was performed at 7 h post infection. The mean ± SEM of four independent experiments is shown. (*B*) Impact of the glycolysis inhibitor 2-DG on RV-B14 replication in HeLa cells and primary human fibroblasts. The mean ± SEM of six independent experiments is shown (*$P < 0.05$, Wilcoxon signed-rank test of normalized data). (*C*) Western blot analysis of capsid protein VP1-3 expression in RV-B14–infected HeLa cells with or without 2-DG treatment. One of two independent experiments performed in duplicates is shown. (*D*) Effect of anaerobic glycolysis inhibition by oxamate on RV reproduction. The mean ± SEM of five independent experiments is shown. (*E*) Impact of the carnitine palmitoyltransferase I inhibitor etomoxir on viral replication in HeLa cells. The mean ± SEM of three independent experiments is shown.

fatty acylcarnitines (butyrylcarnitine, hexanoylcarnitine, myristoylcarnitine, palmitoylcarnitine, and stearoylcarnitine) that were decreased during infection. This was accompanied by decreased levels of various phospholipids, sphingolipids, and ceramides, which, taken together, suggests a shift away from anabolic and lipogenic processes during 2-DG treatment (*SI Appendix*, Fig. S6).

The levels of various nucleotide triphosphates that were increased during infection, including guanosine 5′-triphosphate, guanosine 5′-diphosphate, uridine 5′-triphosphate, uridine 5′-diphosphate, CTP, and cytidine 5′-diphosphate, exhibited a significant decrease during 2-DG treatment (*SI Appendix*, Fig. S6). In conclusion, 2-DG appears to counteract the RV-induced switch toward anabolic metabolism.

2-DG Impairs RV Infection in Vivo. Having established an inhibitory activity of 2-DG in vitro and dissected its mode of action, we were further interested in a therapeutic application of the substance. Therefore, we further studied the possible impact of 2-DG on RV respiratory tract infection in an established murine model (29). In line with our in vitro findings, the substance reduced RV load in infected lung tissue (Fig. 5*A*). Furthermore, virus-induced lung inflammation was reduced by 2-DG, as evidenced by low leukocyte counts in bronchoalveolar lavage (BAL) fluid and decreased bronchiolitis (Fig. 5 *A* and *B*). The mice showed no visible side effects upon treatment with 2-DG, which is in line with previous observations describing the safe use of the substance in various animal models and humans even at much higher doses than used in the present study (30–34). Therefore, 2-DG induced "metabolic starvation" of RVs, which might be considered as a strategy to combat this widespread pathogen.

Discussion

Recent research has established that viruses induce distinct metabolic changes in host cells. The aim of this study was to assess the impact of RV on host cell metabolism, a subject not studied so far to our knowledge.

We found that glucose and fatty acid uptake were up-regulated during infection (Fig. 1 and *SI Appendix*, Fig. S1). Remarkably, the virus-induced enhancement of glucose uptake was measurable as fast as 1.5 h after infection, and was observable throughout 7.5 h in primary human fibroblasts. The velocity of these alterations pointed toward fast adaptation mechanisms such as the known activation of PI3K by RV (19–21). Indeed, an inhibition of this pathway abolished the RV-induced glucose uptake. PI3K is known to modulate glucose uptake through several mechanisms, such as enhancement of vesicle transport (22) and phosphorylation of GLUT1 (23). We found that GLUT1 was rapidly up-regulated upon RV infection and persisted at higher levels until reaching control levels at 7.5 h. This might reflect the beginning of the virus-induced host cell shutdown, resulting in lower levels of host protein synthesis. The still measurable enhancement of glucose uptake at 7.5 h might be mediated through the mentioned phosphorylation of GLUT1 (23), leading to enhanced affinity of the enzyme for glucose.

Consistent with these observations, limiting the glucose supply by depletion of glucose in the culture medium inhibited RV replication. Glutamine, which is utilized as a carbon source by several viruses (1, 4, 5), was also found to be important for RV replication, outlining the necessity of enhanced carbon supply for RV reproduction (Fig. 3*A*).

Metabolomic analysis revealed a specific fingerprint of RV infection. The virus up-regulated glycogenolysis, which is a yet-undescribed mechanism of carbon source generation by viruses

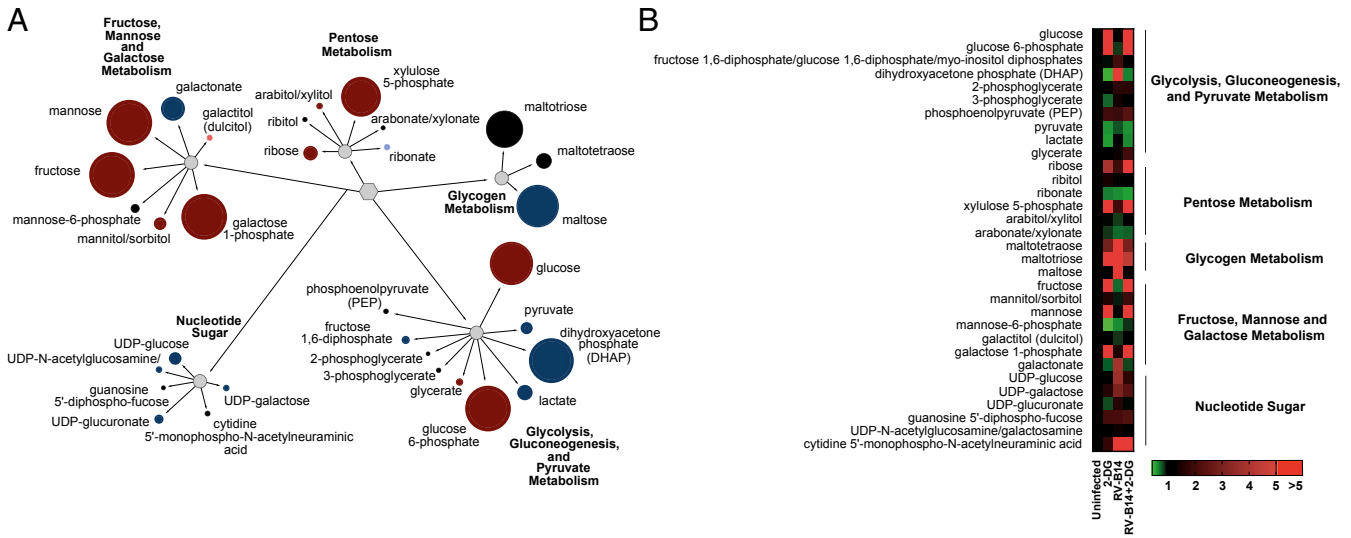

Fig. 4. 2-DG reverts the RV-induced metabolic reprogramming. Metabolomic analysis of HeLa cells infected with RV-B14 (MOI of 3.5) with or without 2-DG treatment. (*A*) The impact of RV infection and the respective changes by 2-DG on carbohydrate metabolism. Colored circles represent statistically significant changes. Dark red circles represent up-regulations; dark blue circles represent down-regulations with $P \leq 0.05$ and fold change >1. Bright red circles represent up-regulations; bright blue circles represent down-regulations with $0.05 < P < 0.10$ and fold change >1. The size of the circles represents the degree of change in 2-DG–treated infected cells compared with untreated infected cells. (*B*) The impact of RV and the respective changes by 2-DG on carbohydrate metabolism in heat map format.

to our awareness. It also enhanced lipogenesis, a process that has been observed for several enveloped viruses such as cytomegalovirus (7, 35, 36), Kaposi sarcoma-associated herpesvirus (37), and hepatitis C virus (38). However, the engagement of this process by a nonenveloped virus was less expected. Although an enhancement of nucleotide availability obviously contributes to viral replication, the induction of lipogenesis serves viral reproduction in a more complex manner. As such, lipids are known to be of importance for the formation of the replication complex that contributes to the generation of membranous vesicles, the sites of virus replication (39). The relevance of these processes for viral replication has been demonstrated via interference with lipid metabolism through inhibition of phosphatidylinositol 4-kinase III-β (40) and fatty acid synthase (41), which both resulted in impaired RV replication.

In line with the observations with glucose-depleted medium, the PGI inhibitor 2-DG abolished RV replication in primary human fibroblasts and in HeLa cells. 2-DG did not elicit measurable effects on cell viability at the concentrations and the time points considered in our infection model. This excludes the possibility that the toxicity of 2-DG might lead to impairment of viral reproduction. Metabolomic analysis revealed that the major alterations induced by RV, i.e., lipogenesis, glycogenolysis, and nucleotide synthesis, were reversed by 2-DG treatment. Additionally, β-oxidation was enhanced as a consequence of the impact of 2-DG on glycolysis, probably to compensate for the bioenergetic requirements. This is likely to cause a skewing of lipid metabolism away from anabolic lipogenesis to fatty acid oxidation, potentially contributing to 2-DG's effects. Therefore, the inhibitory activity of the substance might rely mainly on a shifting of carbon flux to catabolic processes and away from macromolecule production, which is essential for viral replication. In line with this concept, a mere inhibition of energy generation by etomoxir (i.e., β-oxidation) or oxamate (i.e., anaerobic glycolysis) was not sufficient to impair viral reproduction.

Although, to date, 2-DG has been used as an antiviral agent against a variety of viruses in vitro (42), the effect of 2-DG on viral replication has been mostly attributed to its impact on energy homeostasis or interference with protein folding. In the present study, we showed that treatment with mannose did not influence the effect of 2-DG on RV infection, which points toward a negligible role of UPR as the major antiviral mechanism. Furthermore, we show that several strategies of simple energy deprivation are ineffective in impairing RV reproduction. Instead, our data indicate a more complex shift of carbon flux away from anabolic processes, which might be relevant for its antiviral effect toward other viruses (26, 43, 44).

After establishing the RV-impairing effects of 2-DG in vitro, we went on to study the impact of the substance in an established murine infection model (29). We found that 2-DG inhibited viral load and inflammation compared with placebo-treated mice, thus outlining the potential of metabolism-targeting therapy in vivo. Nonetheless, these studies are limited by the marginal resemblance of murine RV infection models to human infection in regard to viral replication level and disease manifestation and kinetics. Therefore, further investigation is warranted to better assess the potential of 2-DG for RV therapy.

Taken together, our findings further highlight the complex interplay between viruses and host cell metabolism and outline these processes as promising targets for specific antiviral therapy. To further confirm our findings, studies in airway epithelial cells and with additional viruses, including clinical isolates and RV-C types, are needed to assess whether metabolic reprogramming is a general characteristic in RV biology.

Materials and Methods

Experimental Model and Subject Details.

Animal experiments. Female C57BL/6 J mice aged 6–8 wk from in-house breeding (originally obtained from The Jackson Laboratory) were used for all experiments. All animal experimentation protocols were evaluated by the animal ethics committee of the Medical University of Vienna and approved by the Ministry of Economy and Science (BMWFW-66.009/0356_WF/V/3b/2015). Animal husbandry and experimentation was performed according to the Federation of Laboratory Animal Science Association guidelines.

Primary cells. For fibroblast isolation, tissue samples including skin and s.c. fat (100–300 cm^2) were obtained from patients undergoing routinely performed body-contouring surgeries and were used for the isolation of mast cells, fibroblasts, and keratinocytes. The skin was inconspicuous upon clinical inspection and on histology. s.c. tissue and reticular dermis were removed, and the remaining split-thickness skin was cut into 0.5-cm^2 pieces and placed

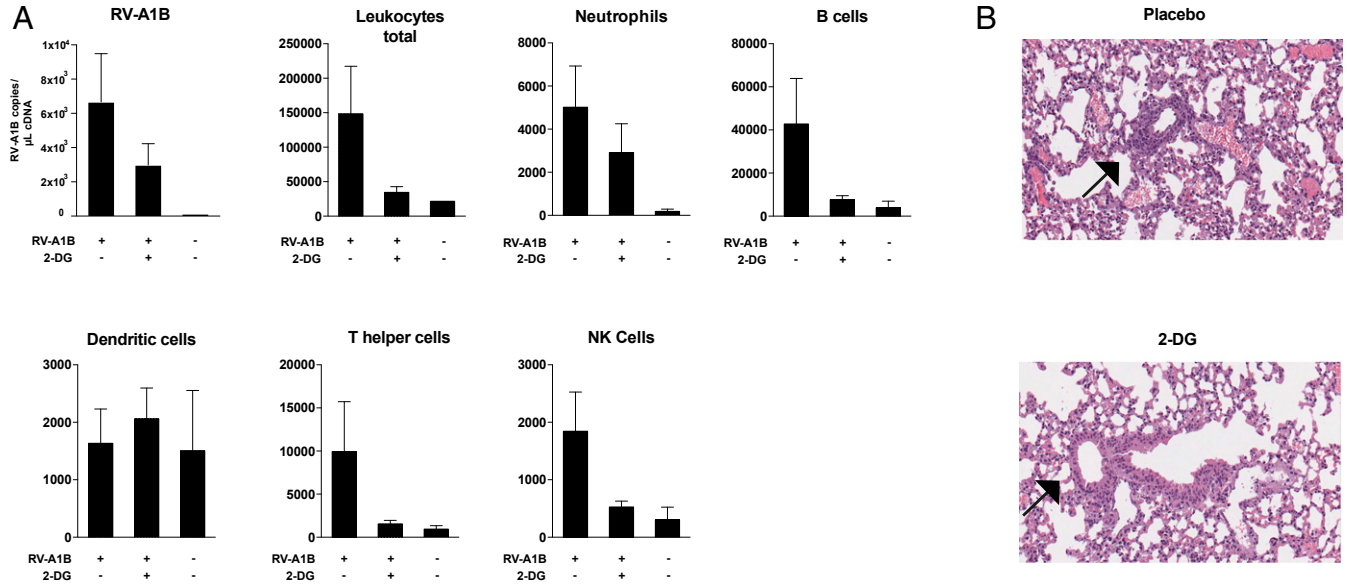

Fig. 5. 2-DG reduces inflammation and viral load in murine RV airway infection. C57BL/6 mice were infected with RV-A1B intranasally plus 50 μL PBS solution (control) or 50 μL of 5 mM 2-DG in PBS solution, respectively. At 24 h after infection, mice were euthanized, a BAL performed, and tissue obtained for qPCR and histological analysis. (*A*) The presence of RV-A1B RNA in lung tissue and the count of leukocyte populations in the BAL (total leukocytes, $CD45^+$; neutrophils, $CD45^+Ly6G^+$; B cells, $CD45^+CD19^+$; dendritic cells, $CD45^+CD11c^+$; T helper cells, $CD45^+CD3^+CD4^+$; NK cells, $CD45^+NK1.1^+$). In each experiment, 10 mice per infection group were used, and two mice were used in the uninfected control group. One of two independent experiments performed is shown. (*B*) Two representative H&E stains of lung tissues of mice treated with PBS solution (placebo) or 2-DG.

overnight at 4 °C in 2.4 U/mL Dispase II (Roche). After the separation of the epidermis, dermis was digested in collagenase I (Gibco) at 37 °C for 2 h. $CD117^+$ mast cells were isolated by using magnetic beads (MACS System; Miltenyi Biotec) according to the manufacturer's instructions. To increase the purity of recovered cells, magnetic isolation was repeated with $CD117^+$ cells from the first isolation round. $CD117^+$ mast cells were then seeded in DMEM (Gibco) supplemented with 10% FCS (Biochrom), penicillin/streptomycin (Biochrom), and 100 ng/mL recombinant human stem cell factor (PeproTech). After the isolation of mast cells, CD117-adherent cells (i.e., fibroblasts) were cultured in supplemented RPMI 1640 with supplements as detailed later (45).

Experiments involving human material were carried out according to the Declaration of Helsinki principles and were approved by the ethics committee of the Medical University of Vienna. Informed written consent was obtained from the participants (vote no. 1149/2011: isolation and culture of cells from and analysis of normal human skin biopsies).

Cell line. HeLa cells (strain Ohio; Flow Laboratories; ECAAC no. 84121901) were cultivated in RPMI 1640 supplemented with 2 mM L-glutamine, (Gibco), 100 U/mL penicillin, 100 μg/mL streptomycin (PAA Laboratories), and 10% FCS (Gibco). For glucose- and glutamine-deprived conditions, RPMI 1640 without glucose or glutamine (both nutrient-deprived media were obtained from PAA Laboratories) plus 10% dialyzed FCS (Thermo Fisher Scientific) and the supplements listed earlier were used. In these experiments, complete RPMI as detailed earlier was used as control with 10% dialyzed FCS.

Methods Details.

Cell culture and in vitro infection. Infection was performed as described before (46). HeLa cells or fibroblasts were plated on polystyrene plates overnight (Corning). On the subsequent day, cells were infected with the indicated amount of 50% tissue culture infective dose ($TCID_{50}$) of RV-B14 per cell [multiplicity of infection (MOI) of 3.5–10]. One hour post infection, cells were washed with prewarmed PBS solution and incubated for 6 h with medium with or without the indicated agent in the indicated concentration before further processing. For assessment of cell viability, cells were stained with the fixable viability dye or 7-AAD (eBioscience) before flow cytometric assessment. For assessment of glucose uptake, cells were infected as described earlier. After the indicated time points, cells were washed with prewarmed PBS solution and coincubated with fluorescently labeled glucose (2-NBDG; Thermo Fisher Scientific) dissolved in PBS solution for 30 min before flow cytometric analysis. For assessment of fatty acid uptake, cells were infected as described previously and coincubated with the labeled fatty acids (C16-Bodipy; Life Technologies) for 6 h before flow cytometric analysis. For analysis of glucose transporter expression, cells were treated as described earlier and stained with anti-GLUT1 Ab (clone 202915; R&D Systems) and anti-GLUT3 Ab (clone 202017; R&D Systems) before flow cytometric measurement.

Metabolomic analyses. HeLa cells were plated, infected, and treated as described earlier (MOI of 3.5) before shock lysis in liquid nitrogen. Metabolomic analysis was performed by Metabolon as follows.

Sample preparation. Samples were prepared by using the automated MicroLab STAR system (Hamilton). Several recovery standards were added before the first step in the extraction process for quality-control (QC) purposes. To remove protein, dissociate small molecules bound to protein or trapped in the precipitated protein matrix, and recover chemically diverse metabolites, proteins were precipitated with methanol under vigorous shaking for 2 min (GenoGrinder 2000; Glen Mills) followed by centrifugation. The resulting extract was divided into five fractions: two for analysis by two separate reverse-phase (RP)/ultra-performance (UP) LC-MS/MS methods with positive ion-mode electrospray ionization (ESI), one for analysis by RP/UPLC-MS/MS with negative-ion mode ESI, one for analysis by hydrophilic interaction liquid chromatography (HILIC)/UPLC-MS/MS with negative-ion mode ESI, and one reserved for backup. Samples were placed briefly on a TurboVap (Zymark) to remove the organic solvent. The sample extracts were stored overnight under nitrogen before preparation for analysis.

Quality assurance. Several types of controls were analyzed in concert with the experimental samples: a pooled matrix sample generated by taking a small volume of each experimental sample (or alternatively, use of a pool of well-characterized human plasma) served as a technical replicate throughout the data set; extracted water samples served as process blanks; and a mixture of QC standards that were carefully chosen not to interfere with the measurement of endogenous compounds were spiked into every analyzed sample, allowed instrument performance monitoring, and aided chromatographic alignment. Instrument variability was determined by calculating the median relative SD (RSD) for the standards that were added to each sample before injection into the mass spectrometers. Overall process variability was determined by calculating the median RSD for all endogenous metabolites (i.e., noninstrument standards) present in 100% of the pooled matrix samples.

UPLC-MS/MS. All methods used a ACQUITY UPLC system (Waters) and a Q-Exactive high-resolution/accurate mass spectrometer (Thermo Fisher Scientific) interfaced with a HESI-II heated ESI source and Orbitrap mass analyzer operated at 35,000 mass resolution. The sample extract was dried and then reconstituted in solvents compatible with each of the four methods. Each reconstitution solvent contained a series of standards at fixed concentrations to ensure injection and chromatographic consistency. One aliquot was analyzed by using acidic positive-ion conditions, chromatographically optimized

for more hydrophilic compounds. In this method, the extract was gradient-eluted from a C18 column (UPLC BEH C18-2.1 × 100 mm, 1.7 μm; Waters) by using water and methanol containing 0.05% perfluoropentanoic acid (PFPA) and 0.1% formic acid (FA). Another aliquot was also analyzed by using acidic positive-ion conditions, but it was chromatographically optimized for more hydrophobic compounds. In this method, the extract was gradient-eluted from the aforementioned C18 column by using methanol, acetonitrile, water, 0.05% PFPA, and 0.01% FA and was operated at an overall higher organic content. Another aliquot was analyzed by using basic negative-ion optimized conditions using a separate dedicated C18 column. The basic extracts were gradient eluted from the column by using methanol and water, but with 6.5 mM ammonium bicarbonate at pH 8. The fourth aliquot was analyzed via negative ionization following elution from an HILIC column (UPLC BEH Amide 2.1 × 150 mm, 1.7 μm; Waters) using a gradient consisting of water and acetonitrile with 10 mM ammonium formate, pH 10.8. The MS analysis alternated between MS and data-dependent MS^n scans by using dynamic exclusion. The scan range varied slightly between methods but covered 70–1,000 *m/z* ratios. Raw data files are archived and extracted as described later.

Data extraction and compound identification. Raw data were extracted, peak-identified, and QC-processed by using Metabolon's hardware and software. These systems are built on a Web-service platform utilizing Microsoft's .NET technologies, which run on high-performance application servers and fiber-channel storage arrays in clusters to provide active failover and load-balancing. Compounds were identified by comparison with library entries of purified standards or recurrent unknown entities. Metabolon maintains a library based on authenticated standards that contains the retention time/index (RI), *m/z* ratio, and chromatographic data (including MS/MS spectral data) on all molecules present in the library. Furthermore, biochemical identifications are based on three criteria: retention index within a narrow RI window of the proposed identification, accurate mass match to the library ±10 ppm, and the MS/MS forward and reverse scores between the experimental data and authentic standards. The MS/MS scores are based on a comparison of the ions present in the experimental spectrum to the ions present in the library spectrum.

Western blot analysis. HeLa cells were infected as described earlier . At 7 h post infection, cells were lysed in 0.5% Triton-X buffer for 5 min on ice. The suspension was centrifuged for 5 min at 13,000 × *g*, and the supernatant was used for further analysis. Western blot analysis was performed as described previously (47). In-house produced rabbit anti-RV VP1-3 antibodies (48) and anti-GAPDH (Cell Signaling Technology) were used at a dilution of 1:1,000. Detection was performed with suitable peroxidase-conjugated secondary antibodies and the Pierce ECL Western blotting substrate (Thermo Fisher Scientific) on an LAS-4000 image analyzer (Fujifilm). Data analysis, quantification, and processing were performed with Fiji (ImageJ) image processing software.

Quantitative real-time PCR. After incubation, cells were lysed and RNA obtained with the RNeasy Kit (Qiagen) according to the manufacturers protocol. The purified RNA was then converted to first-strand cDNA by using the First-Strand cDNA Synthesis Kit (Thermo Fisher Scientific) according to the manufacturer's protocol. Quantitative real-time PCR (qPCR) analysis was performed as described previously (49). For normalization of gene expression, HPRT was used as endogenous control. The Livak method (50) was applied for determination of expression levels of the target gene compared with the endogenous control. All primer sequences are provided in *SI Appendix*, Table S1.

Murine RV infection model. An animal care professional not related to the study performed allocation of mice to the groups randomly. Experiments were performed according to a published protocol (29) with minor modifications. Mice were sedated with isoflurane, and an inoculum of 5×10^6 $TCID_{50}$ of RV-A1B in PBS solution was applied intranasally. Either 5 mM 2-DG dissolved in PBS solution or plain PBS solution (control) was applied simultaneously. After 24 h, mice were euthanized and a BAL was performed. BAL fluid was weighted to estimate volume and centrifuged, and cell count was performed after resuspension. The cells were then stained with the antibodies as stated in the figure legends with antibodies against CD19, NK1.1, CD4, CD45 (BD Bioscience) and Ly6G, and CD11c (BioLegend). After BAL, the chest cavity was opened, and one lung lobe was used for PCR analysis and the other for histological examination. For PCR analysis, the material was homogenized before RNA isolation with the RNeasy kit as described earlier. For histological analysis, lung lobes were fixed in 10% formaldehyde and embedded in paraffin. Lung sections (4 μm) were stained with H&E and evaluated by a pathologist blinded to group allocation.

Quantification and statistical analysis. Regarding metabolomics data, following normalization to Bradford protein concentration, log transformation and imputation of missing values, if any, with the minimum observed value for each compound, ANOVA contrasts, and Welch's two-sample *t* tests were used to identify biochemicals that differed significantly between experimental groups.

All datasets except metabolomics data were organized in Prism (GraphPad). Statistical tests are listed in the figure legends. Normality and homogeneity of variance were used to determine met the assumption of the statistical test used. Significance is defined as $P < 0.05$, and data are depicted as mean ± SEM unless stated otherwise in the figure legend.

ACKNOWLEDGMENTS. We thank Prof. Adelheid Elbe-Bürger for providing human skin fibroblasts, Claus Wenhardt and Alexandra Stieger for excellent technical assistance, and DI Anna Hagen for graphical assistance.

1. Sanchez EL, Lagunoff M (2015) Viral activation of cellular metabolism. *Virology* 479–480:609–618.
2. DeBerardinis RJ, et al. (2007) Beyond aerobic glycolysis: Transformed cells can engage in glutamine metabolism that exceeds the requirement for protein and nucleotide synthesis. *Proc Natl Acad Sci USA* 104:19345–19350.
3. Wise DR, et al. (2008) Myc regulates a transcriptional program that stimulates mitochondrial glutaminolysis and leads to glutamine addiction. *Proc Natl Acad Sci USA* 105:18782–18787.
4. Chambers JW, Maguire TG, Alwine JC (2010) Glutamine metabolism is essential for human cytomegalovirus infection. *J Virol* 84:1867–1873.
5. Fontaine KA, Camarda R, Lagunoff M (2014) Vaccinia virus requires glutamine but not glucose for efficient replication. *J Virol* 88:4366–4374.
6. Fontaine KA, Sanchez EL, Camarda R, Lagunoff M (2015) Dengue virus induces and requires glycolysis for optimal replication. *J Virol* 89:2358–2366.
7. Vastag L, Koyuncu E, Grady SL, Shenk TE, Rabinowitz JD (2011) Divergent effects of human cytomegalovirus and herpes simplex virus-1 on cellular metabolism. *PLoS Pathog* 7:e1002124.
8. Yu Y, Maguire TG, Alwine JC (2011) Human cytomegalovirus activates glucose transporter 4 expression to increase glucose uptake during infection. *J Virol* 85:1573–1580.
9. Thai M, et al. (2014) Adenovirus E4ORF1-induced MYC activation promotes host cell anabolic glucose metabolism and virus replication. *Cell Metab* 19:694–701.
10. Thai M, et al. (2015) MYC-induced reprogramming of glutamine catabolism supports optimal virus replication. *Nat Commun* 6:8873.
11. Bertino JS (2002) Cost burden of viral respiratory infections: Issues for formulary decision makers. *Am J Med* 112(suppl 6A):42S–49S.
12. Blaas D, Fuchs R (2016) Mechanism of human rhinovirus infections. *Mol Cell Pediatr* 3:21.
13. Kirchberger S, Majdic O, Stockl J (2007) Modulation of the immune system by human rhinoviruses. *Int Arch Allergy Immunol* 142:1–10.
14. Kaiser L, et al. (2006) Chronic rhinoviral infection in lung transplant recipients. *Am J Respir Crit Care Med* 174:1392–1399.
15. Liu M, et al. (2010) Long-term impact of respiratory viral infection after pediatric lung transplantation. *Pediatr Transplant* 14:431–436.
16. Papi A, et al. (2006) Infections and airway inflammation in chronic obstructive pulmonary disease severe exacerbations. *Am J Respir Crit Care Med* 173:1114–1121.
17. Steinke JW, Borish L (2016) Immune responses in rhinovirus-induced asthma exacerbations. *Curr Allergy Asthma Rep* 16:78.
18. Ismail S, et al. (2014) Phosphoinositide-3 kinase inhibition modulates responses to rhinovirus by mechanisms that are predominantly independent of autophagy. *PLoS One* 9:e116055.
19. Newcomb DC, et al. (2008) Human rhinovirus 1B exposure induces phosphatidylinositol 3-kinase-dependent airway inflammation in mice. *Am J Respir Crit Care Med* 177:1111–1121.
20. Bentley JK, et al. (2007) Rhinovirus activates interleukin-8 expression via a Src/p110beta phosphatidylinositol 3-kinase/Akt pathway in human airway epithelial cells. *J Virol* 81:1186–1194.
21. Lau C, et al. (2008) Syk associates with clathrin and mediates phosphatidylinositol 3-kinase activation during human rhinovirus internalization. *J Immunol* 180:870–880.
22. Wieman HL, Wofford JA, Rathmell JC, Margolis B (2007) Cytokine stimulation promotes glucose uptake via phosphatidylinositol-3 kinase/Akt regulation of Glut1 activity and trafficking. *Mol Biol Cell* 18:1437–1446.
23. Lee EE, et al. (2015) A protein kinase C phosphorylation motif in GLUT1 affects glucose transport and is mutated in GLUT1 deficiency syndrome. *Mol Cell* 58:845–853.
24. Macintyre AN, et al. (2014) The glucose transporter Glut1 is selectively essential for CD4 T cell activation and effector function. *Cell Metab* 20:61–72.
25. Smith JA (2014) A new paradigm: Innate immune sensing of viruses via the unfolded protein response. *Front Microbiol* 5:222.
26. Leung HJ, et al. (2012) Activation of the unfolded protein response by 2-deoxy-D-glucose inhibits Kaposi's sarcoma-associated herpesvirus replication and gene expression. *Antimicrob Agents Chemother* 56:5794–5803.
27. Gualdoni GA, et al. (2016) The AMP analog AICAR modulates the Treg/Th17 axis through enhancement of fatty acid oxidation. *FASEB J* 30:3800–3809.
28. O'Sullivan D, et al. (2014) Memory CD8(+) T cells use cell-intrinsic lipolysis to support the metabolic programming necessary for development. *Immunity* 41:75–88.

29. Bartlett NW, et al. (2008) Mouse models of rhinovirus-induced disease and exacerbation of allergic airway inflammation. *Nat Med* 14:199–204.
30. Chiaravalli M, et al. (2016) 2-deoxy-d-glucose ameliorates PKD progression. *J Am Soc Nephrol* 27:1958–1969.
31. Laszlo J, et al. (1961) The effect of 2-deoxy-D-glucose infusions on lipid and carbohydrate metabolism in man. *J Clin Invest* 40:171–176.
32. Singh D, et al. (2005) Optimizing cancer radiotherapy with 2-deoxy-d-glucose dose escalation studies in patients with glioblastoma multiforme. *Strahlenther Onkol* 181: 507–514.
33. Kovarik JJ, et al. (2017) Fasting metabolism modulates the interleukin-12/interleukin-10 cytokine axis. *PLoS One* 12:e0180900.
34. Vijayaraghavan R, et al. (2006) Acute toxicity and cardio-respiratory effects of 2-deoxy-D-glucose: A promising radio sensitiser. *Biomed Environ Sci* 19:96–103.
35. Munger J, Bajad SU, Coller HA, Shenk T, Rabinowitz JD (2006) Dynamics of the cellular metabolome during human cytomegalovirus infection. *PLoS Pathog* 2:e132.
36. Munger J, et al. (2008) Systems-level metabolic flux profiling identifies fatty acid synthesis as a target for antiviral therapy. *Nat Biotechnol* 26:1179–1186.
37. Sanchez EL, et al. (2017) Glycolysis, glutaminolysis, and fatty acid synthesis are required for distinct stages of Kaposi's sarcoma-associated herpesvirus lytic replication. *J Virol* 91:e02237-16.
38. Diamond DL, et al. (2010) Temporal proteome and lipidome profiles reveal hepatitis C virus-associated reprogramming of hepatocellular metabolism and bioenergetics. *PLoS Pathog* 6:e1000719.
39. To KKW, Yip CCY, Yuen K-Y (2017) Rhinovirus–from bench to bedside. *J Formos Med Assoc* 116:496–504.
40. Spickler C, et al. (2013) Phosphatidylinositol 4-kinase III beta is essential for replication of human rhinovirus and its inhibition causes a lethal phenotype in vivo. *Antimicrob Agents Chemother* 57:3358–3368.
41. Ohol YM, Wang Z, Kemble G, Duke G (2015) Direct inhibition of cellular fatty acid synthase impairs replication of respiratory syncytial virus and other respiratory viruses. *PLoS One* 10:e0144648.
42. Kang HT, Hwang ES (2006) 2-deoxyglucose: An anticancer and antiviral therapeutic, but not any more a low glucose mimetic. *Life Sci* 78:1392–1399.
43. Maehama T, et al. (1998) Selective down-regulation of human papillomavirus transcription by 2-deoxyglucose. *Int J Cancer* 76:639–646.
44. Wang Y, et al. (2014) Triggering unfolded protein response by 2-deoxy-D-glucose inhibits porcine epidemic diarrhea virus propagation. *Antiviral Res* 106:33–41.
45. Gschwandtner M, et al. (2017) Proteome analysis identifies L1CAM/CD171 and DPP4/CD26 as novel markers of human skin mast cells. *Allergy* 72:85–97.
46. Schrauf C, et al. (2009) The ssRNA genome of human rhinovirus induces a type I IFN response but fails to induce maturation in human monocyte-derived dendritic cells. *J Immunol* 183:4440–4448.
47. Gualdoni GA, et al. (2015) Azithromycin inhibits IL-1 secretion and non-canonical inflammasome activation. *Sci Rep* 5:12016.
48. Neubauer C, Frasel L, Kuechler E, Blaas D (1987) Mechanism of entry of human rhinovirus 2 into HeLa cells. *Virology* 158:255–258.
49. Leitner J, Grabmeier-Pfistershammer K, Majdic O, Zlabinger G, Steinberger P (2011) Interaction of antithymocyte globulins with dendritic cell antigens. *Am J Transplant* 11:138–145.
50. Livak KJ, Schmittgen TD (2001) Analysis of relative gene expression data using real-time quantitative PCR and the 2(-ΔΔ C(T)) method. *Methods* 25:402–408.